IEEE Access
Multidisciplinary ⋮ Rapid Review ⋮ Open Access Journal

Received June 2, 2020, accepted June 14, 2020, date of publication June 24, 2020, date of current version July 6, 2020.

Digital Object Identifier 10.1109/ACCESS.2020.3004722

Optimal Design of IPMSM for Fuel Cell Electric Vehicles Using Autotuning Elliptical Niching Genetic Algorithm

YOUNG-ROK KANG, JI-CHANG SON, AND DONG-KUK LIM, (Member, IEEE)
School of Electrical Engineering, University of Ulsan, Ulsan 44610, South Korea

Corresponding author: Dong-Kuk Lim (ldk8745@ulsan.ac.kr)

This work was supported by the National Research Foundation of Korea (NRF) funded by the Korean Government (Ministry of Science and ICT) under Grant 2019R1F1A1061132.

ABSTRACT To find multimodal solutions for the optimal design of an interior permanent magnet synchronous motor (IPMSM) for fuel cell electric vehicles, an autotuning elliptical niching genetic algorithm is proposed. With conventional autotuning niching genetic algorithms, some peaks are difficult to find because of a circular niche region. The proposed algorithm solves this problem by introducing an elliptical niche. The superior performance of the proposed algorithm is verified using test functions, and it is applied to the optimal design of an IPMSM for fuel cell electric vehicles.

INDEX TERMS Autotuning niching genetic algorithm (ANGA), fuel cell electric vehicle (FCEV), interior permanent magnet synchronous motor (IPMSM), multimodal, niche, pattern search method (PSM).

I. INTRODUCTION

In fuel cell electric vehicles (FCEVs), high power density and efficiency are important design requirements for driving a motor without an engine and to improve fuel efficiency [1]. Interior permanent magnet synchronous motors (IPMSM) have better power density and efficiency than surface permanent magnet synchronous motors or induction motors [2]–[4]. Hence, the IPMSM is suitable for use in FCEVs [5], [6]. In an IPMSM, however, there is a large cogging torque, resulting in noise and vibration [7]. To improve driving comfort and the stable control of electric vehicles, it is necessary to reduce the cogging torque [8].

Since the analysis of an electric machine is nonlinear, it is usually analyzed using the finite element method (FEM). However, the FEM requires a lot of time to analyze electrical machines [9]. Especially, the analysis of an IPMSM takes more time because the current phase angle at maximum torque per ampere differs with motor shape. To solve this problem, various optimization algorithms have been studied.

Multimodal Optimization (MO) is the useful method which find all or most of multiple solutions and particularly suitable for design of the IPMSM whose cogging torque usually consists of multiple solutions [10]. In recent years, The MO employing niche concept have been researched [1]. However, an excessive application of the niche concept reduces the advantage from searching multiple optimal points [11]. The conventional autotuning niching genetic algorithm (ANGA) using the niche concept has problem of omitting local optimal points in certain circumstances.

To solve this problem, an autotuning elliptical niching genetic algorithm (ANEGA) is proposed in this paper. The AENGA uses an elliptical niche region instead of the conventional circular niche region to avoid omission of multiple peaks within the same niche region. By using the elliptical niche region, the proposed algorithm can find most local optima, improving the search performance of the algorithm. Furthermore, a direct convergence method is invented to reduce the number of function calls, and Latin hypercube sampling and advanced mutation method is introduced to more efficiently search undiscovered optimal points.

The outstanding performance of AENGA was verified by applying it to test functions. Compared to the conventional algorithm ANGA, the AENGA finds more peaks with few function calls. It means that the AENGA can find various solutions when applying it to electric motor design. Based on the various solutions, the best solution satisfying diverse

The associate editor coordinating the review of this manuscript and approving it for publication was Shihong Ding.

requirements such as rated torque, cogging torque, etc. can be found. We applied the AENGA to optimizing the design of an IPMSM to find multiple solutions with less cogging torque. Among the solutions found, the final solution was determined by considering the average torque and torque ripple.

This paper is organized as follows. The conventional multimodal algorithm, ANGA is reviewed in Section II, and Section III describes the proposed methodology. Section IV shows the verification of search performance comparing conventional and proposed algorithm in test functions. Section V describes a motor for FCEV applied to the AENGA and the result. Finally, the conclusions are given in Section VI.

II. CONVENTIONAL OPTIMIZATION ALGORITHM

A. PATTERN SEARCH METHOD

The pattern search method (PSM) is a deterministic optimization algorithm that recycles the path of the previous step. The PSM includes exploratory and pattern movement [13]. During exploratory movement, each sample moves in the direction of increasing fitness, and the vector sum of the exploratory move is defined as a pattern. In the pattern movement step, each sample moves in the direction of the pattern. Figure 1 shows the concept of the PSM. The initial point, u_0, moves to u_1 through two exploratory movements. Then, u_1 moves to u_2 using the pattern of the previous step. Figure 2 shows a flow chart describing the PSM.

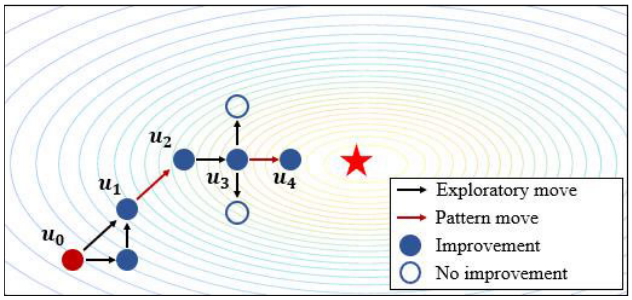

FIGURE 1. The concept of the pattern search method.

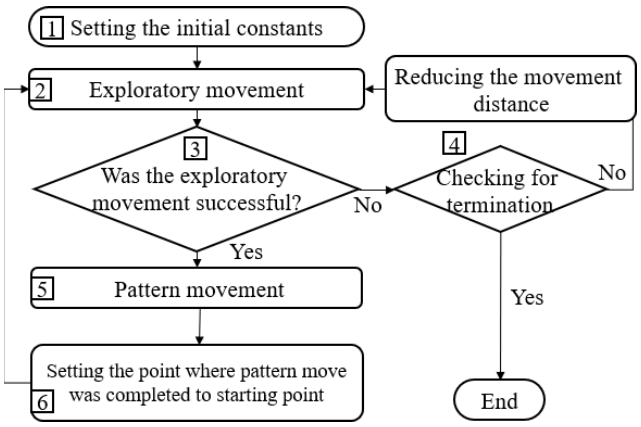

FIGURE 2. The flow chart of the PSM.

Initial samples, the initial movement interval, and the reduction factor for decreasing the movement interval are defined in Step 1.

If the movement interval is less than the criterion, the PSM is terminated in Step 4. Otherwise, the movement interval is decreased by the reduction factor and the process goes to Step 2.

In Step 5, the pattern move proceeds as follows:

$$u_p^{k+1} = u^k + (u^k - u^{k-1}) \tag{1}$$

where u_p^{k+1} is the sample after the pattern move process and $(u^k - u^{k-1})$ is the pattern. In Step 6, u_p^{k+1} is set to the starting point for the next iteration if the following condition is satisfied. Otherwise, the starting point is u^k.

$$f(u_p^{k+1}) > f(u^k) \tag{2}$$

where $f(u_p^{k+1})$ is the fitness of u_p^{k+1} and $f(u^k)$ is the fitness of $f(u^k)$.

B. NICHE REGION

ANGA is a multimodal optimization based on a genetic algorithm (GA). The GA converges only to a global optimal point. However, by introducing a niche region, ANGA can search for multiple local optimal points. Biologically, the niche region represents a group of similar individuals. In this paper, a niche region represents a circular region of the optimal solution as shown in Figure 3. By removing the samples generated within the niche region, it is possible to find multiple optimal points and eliminate unnecessary function calls. The radius of the niche region is determined by the farthest samples that find the same optimal solutions as illustrated in Figure 3. In the following iteration, if there are farther samples, the radius of the niche region is automatically renewed based on these samples.

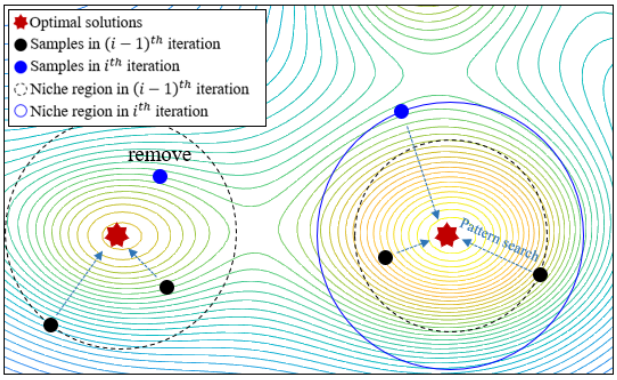

FIGURE 3. Creation and renewal of the niche region and removal of unnecessary sample in ANGA.

C. DRAWBACK OF CONVENTIONAL ANGA

ANGA is an efficient optimization algorithm when the optimal points are evenly distributed. However, it has a missed-peak problem in which some optimal points are omitted when there is an uneven distribution of local peaks as

shown in Figure 4. If there is a valley (Point 1) or the initial sample is at the edge of the design area (Point 2), the niche radius is abnormally large because the search path of the PSM is long. The purple points in Figure 4 are included in another niche radius. Therefore, it is difficult to find all local peaks and the performance of ANGA is degraded.

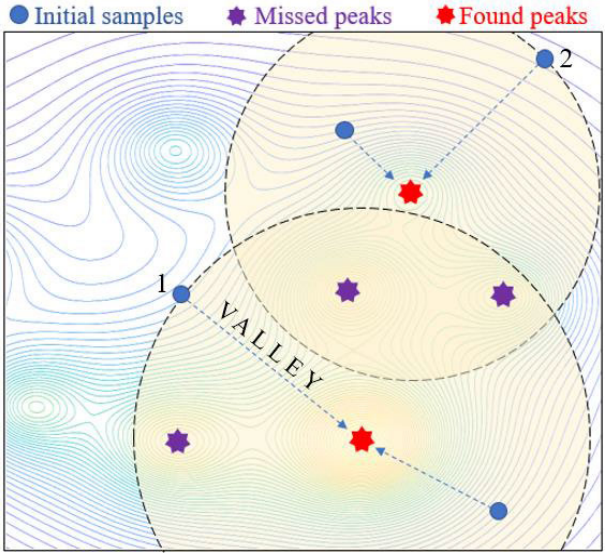

FIGURE 4. The drawback of ANGA.

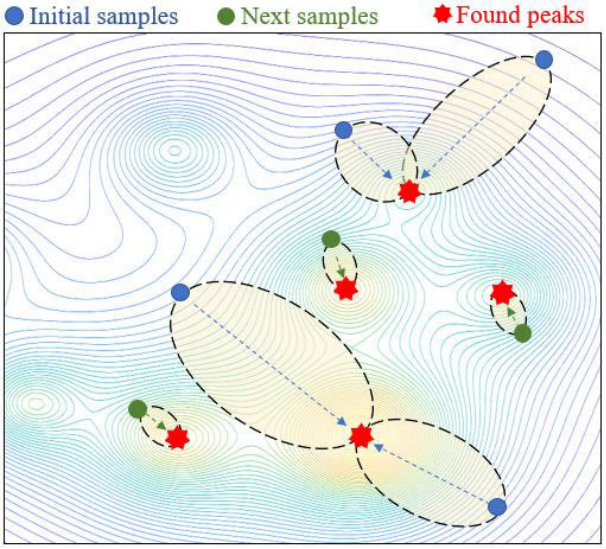

FIGURE 5. The concept of AENGA.

III. PROPOSED OPTIMIZATION ALGORITHM

A. INTRODUCTION OF ELLIPTICAL NICHE RGION

In the proposed algorithm, AENGA, the missed-peak problem is solved by the introduction of an elliptical niche region. As shown in Figure 5, it is possible to create a niche region without including other optimal points since the path of the PSM process is defined as the niche region. The conventional niche region includes other optimal points as illustrated in Figure 4, while the elliptical niche region does not include other peaks as shown in Figure 5. Therefore, the use of AENGA can reduce the number of missed peaks.

B. DIRECT CONVERGENDE METHOD

The AENGA can be considered an inefficient algorithm in terms of the number of function calls because the niche region of AENGA is smaller than that of ANGA. However, when using AENGA, the number of function calls is minimized in the PSM process. When a sample is included in some niche region, the samples directly converge at the optimal point to which each region belongs. It is called direct convergence method. In the same situation, ANGA continues searching for an optimal point. Hence, AENGA can reduce the number of function calls even though it uses a smaller niche region.

C. GENERATION OF INITIAL SAMPLES USING LATIN HYPERCUBE SAMPLING (LHS)

It is important to evenly locate the initial solutions because we cannot know the location of the optimal points in the problem region. When using a general sampling method, it is difficult to evenly locate the initial samples over the entire problem region. Latin hypercube sampling (LHS) is a method which scatters samples evenly by considering the distance between them as shown in Figure 6.

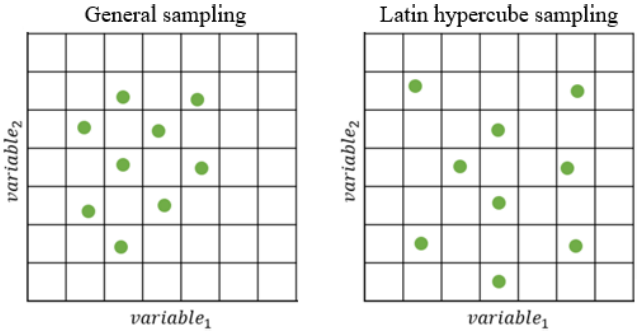

FIGURE 6. The comparison between general sampling and the LHS.

D. ADVANCED MUTATION METHOD

As AENGA progresses, samples are generated near the global optimal point. Mutation is a means of finding regions that have not yet been searched. In the general mutation method, mutations are randomly generated across the whole problem region. However, function calls can be wasted since the general method may repeatedly explore already-searched regions.

In this paper, an advanced mutation method is introduced to generate mutations in regions far from the cluster of samples as shown in Figure 7 [14]. The formula determining the distance between the sample and the cluster of samples is as

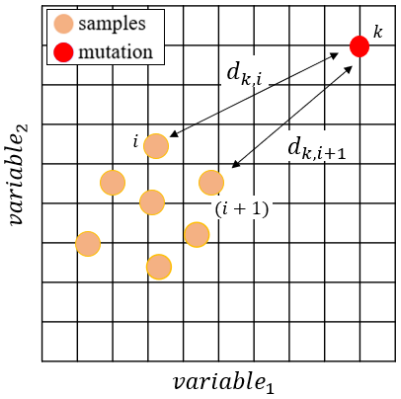

FIGURE 7. The advanced mutation method based on the average Euclidean-distance.

follows:

$$D_k = \frac{\sum_{i=1}^{N_p} d_{k,i}}{N_P} \tag{3}$$

where D_k is the average Euclidean distance between the k^{th} mutation and the samples, N_p is the number of samples, and $d_{k,i}$ is the Euclidean distance between the k^{th} mutation and the i^{th} samples. The high value of D_k means that the k^{th} mutation is far from the cluster. By generating mutations with a high value of D_k, the advanced mutation method avoids duplicate searches and explores unfound regions.

E. FLOW CHART FOR AENGA

The flow chart for AENGA is shown in Figure 8.

Step 1. Setting the Initial Values Using LHS

Initial samples are generated in the design area using the LHS method.

Step 2. Pattern Search Method

The pattern search method is applied to each sample to find optimal points.

Step 3. Generation of Elite Set

An elite set is a set of optimal points with high fitness. The optimal points found in the PSM process are stored in the elite set.

Step 4. Generation of Elliptical Niche Region

The elliptical niche regions are generated. The major axis and minor axis are defined as follows:

$$\begin{aligned} a &= \left| eliteset_i - individuals_{i,k} \right| \\ b &= a/3 \end{aligned} \tag{4}$$

where a is the major axis, $eliteset_i$ is the i^{th} element of the elite set, $individual_{i,k}$ is the k^{th} initial sample of the PSM process that found $eltieset_i$, and b is the minor axis.

Step 5. Selection of Parents Population

The parents population is selected to create the next generation using the roulette wheel method.

Step 6. Generation of Child Samples.

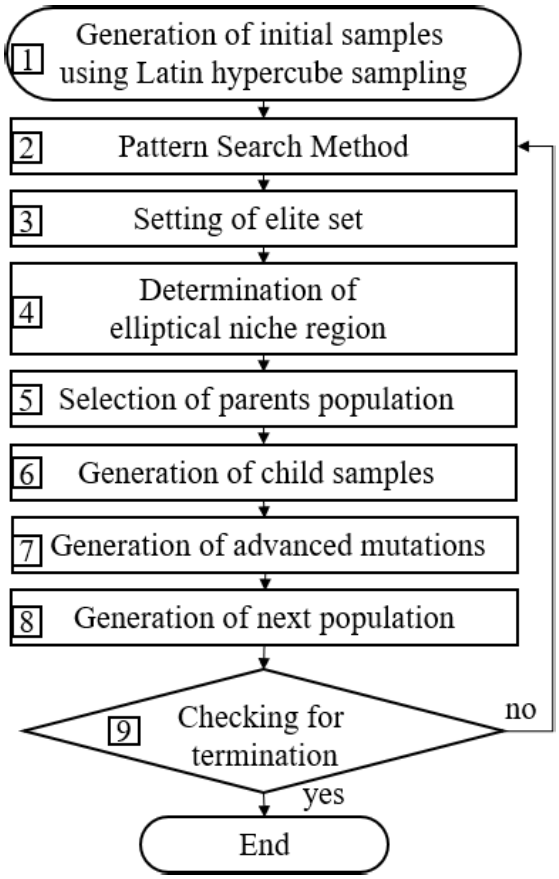

FIGURE 8. The flow chart for AENGA.

Child samples are generated using the parent population and the following equation

$$P_{child} = (P_{parent1} + P_{parent2})/2 \tag{5}$$

where P_{child} is a child sample, and where $P_{parent1}$ and $P_{parent2}$ are a pair of parent samples. The number of child populations is automatically adjusted to double the elite set.

Step 7. Generation of Advanced Mutation.

Advanced mutations are generated using the Euclidian distance.

Step 8. Generation of Next Population.

If child samples or mutations are included in the elliptical niche region, they are excluded from the candidates and regenerated by the number of excluded samples.

Step 9. Checking for Convergence.

If the found peaks are not changed during four iterations, the AENGA is terminated. Otherwise, the process goes to step 2.

IV. TEST FUNCTION

Test functions are used to demonstrate the effectiveness of AENGA, and are described as follows:

$$f(x, y) = \sum_{k=1}^{N_P} \frac{b_k}{1 + \frac{(x-x_{pk})^2 + (y-y_{pk})^2}{a_k}} \tag{6}$$

TABLE 1. Result Of Comparison between ANGA and AENGA.

Test Function 1 [8 Peaks]	Number of Function calls	Success rate [%]
ANGA	1641	84.5
AENGA	1618	97.5
Test Function 2 [36 Peaks]	**Number of Function calls**	**Success rate [%]**
ANGA	3480	92.4
AENGA	3414	96.4

where N_p is the number of peaks, a_k is the width of the k^{th} peak, and x_{pk} and y_{pk} describe the position of the k_{th} peak, respectively. The results of repeating each algorithm 100 times are shown in Table 2. In test function 1, the number of function calls is 1424 in ANGA and 1658 in AENGA. The success rate, which is the ratio of the number of peaks found to the total number of peaks, is 82.5% in ANGA and 97.5% in AENGA. In test function 2, the number of function calls is 3480 in ANGA and 3414 in AENGA. The success rate is 92.4% in ANGA and 96.4% in AENGA.

TABLE 2. Requirement specifications.

	Value	Unit
Pole/slot/phase	6/27/3	-
Stator inner/outer diameter	16/58	mm
Rotor inner/outer diameter	170/50	mm
Axial length	230	mm
Permanent magnet	NEOMAX-42	-
Rated torque	310	Nm
Voltage limit	124.7	V
Current limit	650	A
Rpm	3,000	r/m
Rated power	97.4	kW
Cogging torque	3	Nm
Torque ripple	10	%

Although both algorithms have a similar number of function calls, AENGA clearly has a better success rate. This shows that the proposed algorithm can find more optimal points with fewer function calls than the conventional algorithm.

V. SELECTED MODEL FOR FCEV

A. REQUIREMENTS AND SPECIFICATION OF IPMSM FOR FCEV

IPMSMs are suitable for use as FCEV motors because of their high torque density and efficiency. However, the high cogging torque and torque ripple of the IPMSM causes noise and vibration, resulting in decreased control stability and driving comfort. In order to minimize the cogging torque and to consider the average torque and torque ripple, the proposed

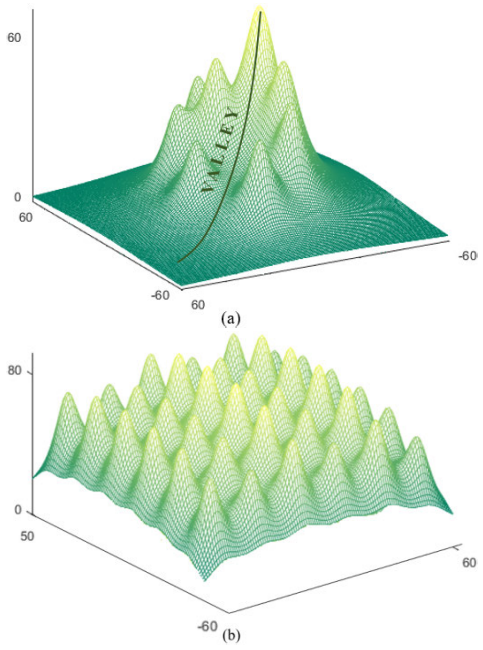

FIGURE 9. The test functions: (a) with eight peaks, and (b) with 36 peaks.

AENGA is applied to the optimal design of an IPMSM for use in FCEVs.

In contrast to HEV, FCEV has a large capacity from 80 to 160 kW because it uses only an electric motor to drag the vehicle. Since the electric motors are arranged alone without engine, there is enough space. Therefore, the cylinder type and the distributed winding method usually applied to the motor for FCEV in order to satisfy required output power and torque ripple. The IPMSM in this study also satisfied the requirements by applying the distributed winding and cylinder type.

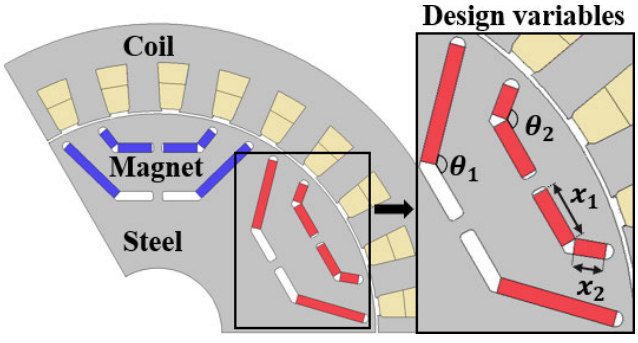

FIGURE 10. The benchmarked model for FCEV.

The topology and requirements are shown in Figure 10 and Table 2. The rated torque is 318 Nm and rated power is 97.4 kW at 3,000 RPM. The permanent magnet is a NEOMAX-42 with a magnetic flux density of 1.14 T.

The initial model is a three-phase, six-pole, 27-slot electric motor. Generally, if the number of poles and slots increase, the torque also increases because the overall

saturation of magnetic flux density becomes uniform. Since FCEVs require a high-power density, multipolar rotor is recommended. However, for stable control, a switching frequency should be at least 15 times than the electric frequency at the maximum speed. Considering this condition, 6 poles were selected for an application model. The 27, 36, 54 slots are available for the 6 poles motor, and the 27 slots which have minimum cogging torque were selected for the application model [15].

In the FCEV motor, the power is supplied from the fuel cell and the DC link voltage is in the range of 240 to 450V. In order to ensure stable driving performance of the motor, the lowest 240 V was considered for the limitation. In this paper, Space Vector Pulse Width Modulation (SVPWM), which has high voltage utilization, is used, and a voltage margin of 10 % is set to maintain instantaneous current control. Phase voltage limit are determined to 124.7 V by formula (7), and phase current limit are determined to 650 A by formula (8) when the maximum input power is 110 kW and the power factor is 0.9 [15].

$$V_{\max} = \frac{V_{dc}}{\sqrt{3}}(0.9) \tag{7}$$

$$I_{\max} = \frac{2}{3}\frac{P_{in}}{V_{\max}\cos\varphi} \tag{8}$$

V_{max} is the phase voltage limit and V_{dc} is the minimum DC link voltage. I_{max} is the phase current limitation. P_{in} is input power and $cos\ \varphi$ is a power factor. The optimal model of this study is designed to satisfies these limitations.

To operate the motor with thermal stability, it is necessary to determine the proper current density. The current density is determined by the cooling method, operation time, insulation level, and etc. In this paper, it was decided as 10 A/mm^2 considering water cooling, 30 second maximum rated operation, and N class insulation at 200°.

B. DESIGN VARIABLES AND OBJECTIVE FUNCTION

Cogging torque reduction is an important aspect of electrical motor design because it is directly connected to noise and vibration. Therefore, the cogging torque is selected as the objective function, and the torque ripple and average torque are also considered. The cogging torque and torque ripple can be reduced by adjusting the topology of the rotor [16], [17]. This determines the selection of the angles and lengths of the magnets as design variables in Figure 10. Their ranges are determined by considering the manufacturing process as following:

$$\begin{aligned} 120^\circ &\le \theta_1 \le 140^\circ \\ 120^\circ &\le \theta_2 \le 150^\circ \\ 5mm &\le x_1 \le 20mm \end{aligned} \tag{9}$$

where θ_1 is the angle between the first-floor magnets and θ_2 is the angle between the second-floor magnets. The thickness of the bridge is kept constant to ensure instrument stability when changing the design variables, and x_2 is determined by the thickness of the bridge and θ_2.

TABLE 3. Optimal design results.

	Initial model	Case1	Case2	Case3	Unit
θ_1	131	122	131.3	129	°
θ_2	142	141.8	128.3	131	°
x_1	11	8	11.5	17	mm
x_2	8.8	9.7	7.5	6.3	mm
Cogging torque	13.28	0.3	0.83	0.96	Nm
Torque ripple	5.9	19.2	5.2	21.7	%
Average torque	314.2	307.1	313.5	321.6	Nm

C. RESULTS FOR THE OPTIMAL DESIGN

Table 3 shows the results of applying AENGA to the conventional model for reducing cogging torque. The initial model has a cogging torque of 13.28 Nm, a torque ripple of 5.9%, and average torque of 314.2 Nm. There are three main results from the optimization. First, Case1 has the lowest cogging torque of the three cases. However, Case1 is not appropriate for the final design because it has a high torque ripple of 19.2% and a low average torque of 307.1 Nm. Second, Case2 has a low cogging torque of 0.83 Nm with a decreased torque ripple of 5.2% and a high average torque of 313.5 Nm. Finally, Case3 also has a low cogging torque of 0.96 Nm and the highest average torque of 321.6 Nm. However, the torque ripple is 21.7%. Of the three cases, only Case2 satisfies the requirements. Therefore, Case2 is selected as the final optimization model of the IPMSM for FCEVs.

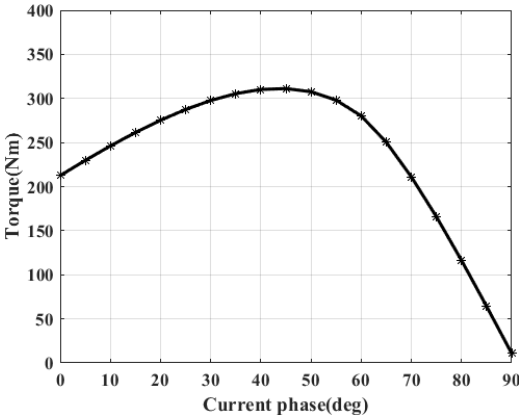

FIGURE 11. The MTPA of the optimal model.

Figure 11 shows the FEM results for finding the maximum torque per ampere (MTPA). Based on these results, the current phase angle is set to 44°. Figure 12 shows the flux density distribution. Figure 13 shows the cogging torque waveform comparison between the initial model and the optimized model. Figure 14 shows the reduction of torque ripple in the rated condition. Compared to the initial model, the cogging torque of the optimal model was reduced by 98%, and the torque ripple was reduced by 12%.

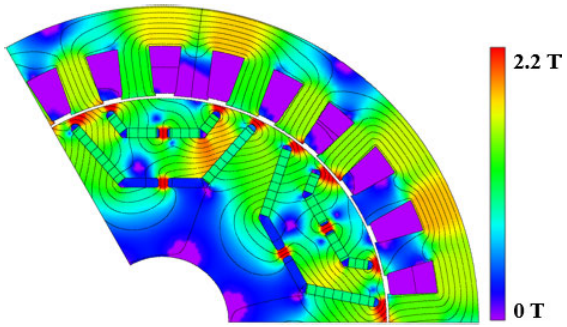

FIGURE 12. The flux density of the optimal model.

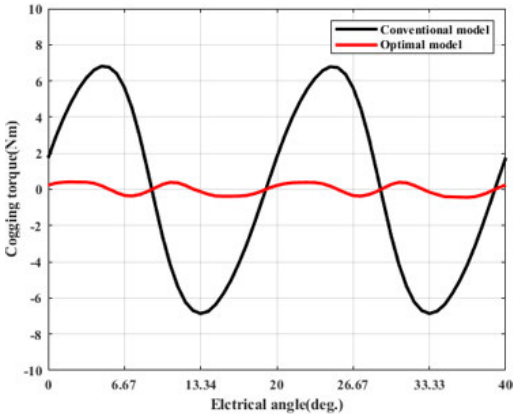

FIGURE 13. Comparison of the cogging torque.

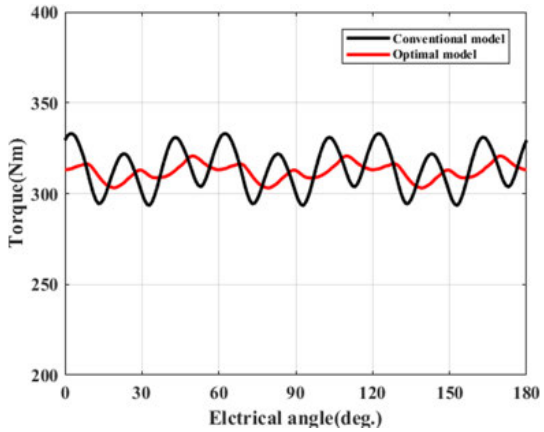

FIGURE 14. Comparison of the torque.

In an IPMSM, it is essential to analyze the stress caused by the centrifugal force of the rotor at high rotational speeds. The maximum speed of the optimal model is 12,000 RPM, the analysis of which was performed under the conditions tabulated in Table 5. Figure 15 shows the result of the stress analysis. The maximum stress is 110 MPa near the center post and does not exceed the yield point of the rotor core, 250 MPa. Therefore, the optimal model is safe from breakage even when rotating at high speed.

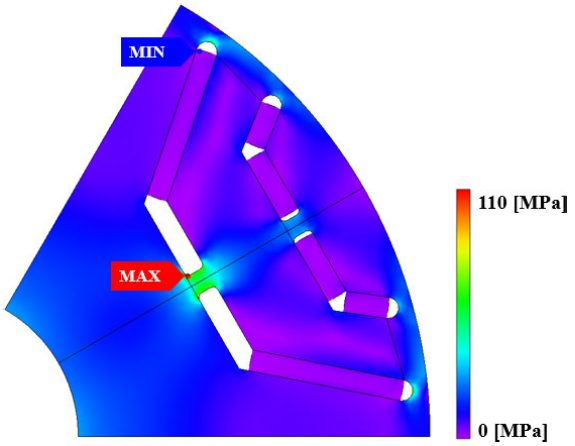

FIGURE 15. Von Mises stress of the optimal model.

TABLE 4. Conditions for stress analysis.

Section	Value
Young's modulus (Core / PM) [GPA]	200 / 120
Poisson's ratio (Core / PM)	0.3 / 0.3
Density (Core / PM)	7850 / 8400
Yield point of core [MPa]	250
Speed [RPM]	12,000

VI. CONCLUSION

In this paper, we proposed AENGA for multimodal optimization. The missed-peak problem encountered when using the conventional algorithm was solved by introducing an elliptical niche region. The proposed AENGA was able to find the global optimal point as well as local optimal points with a small number of function calls. Its outstanding performance was verified by comparison with the conventional ANGA using test functions. Furthermore, AENGA was applied to the optimal design of an IPMSM for use in FCEVs. The objective was the reduction of the cogging torque, as well as improvement of the torque ripple and average torque performance using various optimal points. Based on these advantages, the proposed AENGA is expected to be widely used for the optimal motor design that needs to consider various performance factors. As a future work, we will conduct a study on increasing design variables of the AENGA to find a variety of optimal solutions considering various constructions.

REFERENCES

[1] J.-G. Lee, D.-K. Lim, and H.-K. Jung, "Analysis and design of interior permanent magnet synchronous motor using a sequential-stage magnetic equivalent circuit," *IEEE Trans. Magn.*, vol. 55, no. 10, pp. 1265–1268, Oct. 2019.

[2] D.-K. Lim, K.-P. Yi, S.-Y. Jung, H.-K. Jung, and J.-S. Ro, "Optimal design of an interior permanent magnet synchronous motor by using a new surrogate-assisted multi-objective optimization," *IEEE Trans. Magn.*, vol. 51, no. 11, Nov. 2015, Art. no. 8207504.

[3] S. Lee, Y.-S. Jeong, Y.-J. Kim, and S.-Y. Jung, "Novel analysis and design methodology of interior permanent-magnet synchronous motor using newly adopted synthetic flux linkage," *IEEE Trans. Ind. Electron.*, vol. 58, no. 9, pp. 3806–3814, Sep. 2011.

[4] G. Hong, T. Wei, and X. Ding, "Multi-objective optimal design of permanent magnet synchronous motor for high efficiency and high dynamic performance," *IEEE Access*, vol. 6, pp. 23568–23581, Apr. 2018.
[5] J. Wu, J. Wang, C. Gan, Q. Sun, and W. Kong, "Efficiency optimization of PMSM drives using field-circuit coupled FEM for EV/HEV applications," *IEEE Access*, vol. 6, pp. 15192–15201, 2018.
[6] H. Li, X. Zhang, S. Yang, E. Li, and J. Hong, "Multi-objective controller design of IPMSM drives based on DTD D-Partition method considering parameters uncertainties," *IEEE Trans. Energy Convers.*, vol. 34, no. 2, pp. 1052–1062, Jun. 2019.
[7] K.-C. Kim, "A novel method for minimization of cogging torque and torque ripple for interior permanent magnet synchronous motor," *IEEE Trans. Magn.*, vol. 50, no. 2, pp. 793–796, Feb. 2014.
[8] D.-W. Kim, G.-J. Park, J.-H. Lee, J.-W. Kim, Y.-J. Kim, and S.-Y. Jung, "Hybridization algorithm of fireworks optimization and generating set search for optimal design of IPMSM," *IEEE Trans. Magn.*, vol. 53, no. 6, Jun. 2017, Art. no. 8106404.
[9] C.-H. Yoo, D.-K. Lim, D.-K. Woo, J.-H. Choi, J.-S. Ro, and H.-K. Jung, "A new multimodal optimization algorithm for the design of in-wheel motors," *IEEE Trans. Magn.*, vol. 51, no. 3, Mar. 2015, Art. no. 8201704.
[10] C.-H. Yoo, D.-K. Lim, and H.-K. Jung, "A novel multimodal optimization algorithm for the design of electromagnetic machines," *IEEE Trans. Magn.*, vol. 52, no. 3, Mar. 2016, Art. no. 8201304.
[11] H.-J. Park, H.-K. Yeo, S.-Y. Jung, T.-K. Chung, J.-S. Ro, and H.-K. Jung, "A robust multimodal optimization algorithm based on a sub-division surrogate model and an improved sampling method," *IEEE Trans. Magn.*, vol. 54, no. 3, Mar. 2018, Art. no. 8201704.
[12] D.-H. Cho, J.-K. Kim, H.-K. Jung, and C.-G. Lee, "Optimal design of permanent-magnet motor using autotuning niching genetic algorithm," *IEEE Trans. Magn.*, vol. 39, no. 3, pp. 1265–1268, May 2003.
[13] J.-K. Kim, D.-H. Cho, H.-K. Jung, and C.-G. Lee, "Niching genetic algorithm adopting restricted competition selection combined with pattern search method," *IEEE Trans. Magn.*, vol. 38, no. 2, pp. 1001–1004, Mar. 2002.
[14] J. H. Lee, J.-W. Kim, J.-Y. Song, D.-W. Kim, Y.-J. Kim, and S.-Y. Jung, "Distance-based intelligent particle swarm optimization for optimal design of permanent magnet synchronous machine," *IEEE Trans. Magn.*, vol. 53, no. 6, Jun. 2017, Art. no. 7206804.
[15] S. Y. Gwak, "Characteristic analysis and design of multi-layer buried permanent magnet motor for vehicle traction," Ph.D. dissertation, Dept. Elect. Eng., Seoul National Univ., Seoul South Korea, 2008.
[16] J. Hao, S. Suo, Y. Yang, Y. Wang, W. Wang, and X. Chen, "Optimization of torque ripples in an interior permanent magnet synchronous motor based on the orthogonal experimental method and MIGA and RBF neural networks," *IEEE Access*, vol. 8, pp. 27202–27209, Feb. 2020.
[17] L. Fang, S.-I. Kim, S.-O. Kwon, and J.-P. Hong, "Novel double-barrier rotor designs in interior-PM motor for reducing torque pulsation," *IEEE Trans. Magn.*, vol. 46, no. 6, pp. 2183–2186, Jun. 2010.

YOUNG-ROK KANG received the B.S. degree in electrical engineering from the School of Electrical Engineering, University of Ulsan, South Korea, in 2019, where he is currently pursuing the M.S. degree.

His research interest includes analysis and optimal design of electrical machines.

JI-CHANG SON received the B.S. degree in electrical engineering from the School of Electrical Engineering, University of Ulsan, South Korea, in 2019, where he is currently pursuing the M.S. degree.

His research interest includes analysis and optimal design of electrical machines.

DONG-KUK LIM (Member, IEEE) received the B.S. degree in electrical engineering from Dongguk University, Seoul, South Korea, in 2010, and the Ph.D. degree in electrical engineering from Seoul National University, Seoul, through the Combined master's and Ph.D. Program, in 2017.

In 2017, he was with the Electrical Power Engineering Team, Hyundai Mobis Company, South Korea, as a Senior Research Engineer. He is currently an Assistant Professor with the School of Electrical Engineering, University of Ulsan, South Korea. His research interest includes analysis and optimal design of electrical machines.